RSC Advances

PAPER

View Article Online
View Journal | View Issue

Cite this: *RSC Adv.*, 2025, **15**, 45071

Carbon dot-based polyplexes with cell penetration peptides for gene transfection

Hani Nasser Abdelhamid, [a] Ülo Langel,[bc] Mahmoud M. Abdelnaby [d] and Moataz Dowaidar *[de]

This study explores the synthesis, characterization, and gene-delivery efficacy of polyplexes comprising carbon nanomaterials, namely, graphene oxide quantum dots (GO QDs) and carbon dots (CDs), in conjunction with cell-penetrating peptides (CPPs), namely, PF14 or PF221, alongside gene therapeutic agents (pGL3 plasmids or splice-correcting oligonucleotides (SCO)). GO QDs were created using Hummers' method, followed by acid fragmentation, while CDs were generated by an eco-friendly solvothermal procedure utilizing ascorbic acid as a precursor. Structural and morphological characterization using X-ray diffraction (XRD), transmission electron microscopy (TEM), and zeta potential analysis confirmed the synthesis of nanocomplexes with distinct physicochemical properties. Gene transfection assays demonstrated that PF14–CD polyplexes attained superior efficiency in delivering pGL3 and SCO, surpassing GO QDs and PF221-based methods. Mechanistic studies revealed that the cellular uptake of PF14–SCO–CDs is predominantly mediated by scavenger receptor class A (SCARA), as evidenced by the significant inhibition observed with SCARA-specific inhibitors. The use of PF14 and CDs presents a promising model for efficient gene transport, primarily governed by receptor-mediated endocytosis.

Received 2nd September 2025
Accepted 30th October 2025

DOI: 10.1039/d5ra06584d

rsc.li/rsc-advances

Introduction

Zero-dimensional (0D) carbon nanomaterials, specifically graphene quantum dots (GQDs)[1–3] and carbon dots (CDs),[4–7] have emerged as promising candidates in nanotechnology due to their distinctive size-dependent optical, electrical, and physicochemical properties. They exhibit nanoscale carbon structures with particle diameters under 10 nm, leading to quantum confinement and edge effects that improve fluorescence, enhance biocompatibility, confer chemical stability, and increase aqueous solubility.[1] GQDs are graphene sheets with lateral dimensions under 10 nm, typically consisting of several graphene layers.[2] Their synthesis can be categorized into "top-down" and "bottom-up" methodologies. Top-down procedures entail deconstructing larger carbon structures, such as graphene oxide, carbon fibers, or carbon nanotubes, through processes like chemical oxidation, electrochemical exfoliation, or laser ablation. Conversely, bottom-up methodologies fabricate GQDs from molecular precursors using organic synthesis, hydrothermal, or microwave-assisted techniques, providing enhanced control over dimensions, morphologies, and surface characteristics.[3–6] CDs are quasi-spherical, amorphous-to-nanocrystalline carbon nanoparticles recognized for their superior photoluminescence and minimal toxicity.[7] They are often generated through the hydrothermal,[8] solvothermal, or microwave-assisted carbonization of organic precursors, such as vitamins, sugars, metabolites, or natural biomass.[8,9] These synthesis methods are straightforward, economical, and environmentally friendly, rendering CDs suitable for large-scale manufacture.[10] GQDs and CDs have numerous uses in the biomedical sector.[11] Their adjustable photoluminescence and biocompatibility facilitate applications in photocatalysis,[12] bioimaging,[13] drug/gene delivery,[14,15] sensors,[16] biosensing,[17,18] imaging,[19] and photothermal and photodynamic treatments.[20] CDs are extensively utilized in the fluorescence labeling and detection of biological molecules due to their stable and intense luminescence.[21] CDs have also been reported for use in electrocatalysis, offering unique electrochemical properties.[22]

Gene therapy has evolved into a revolutionary approach for addressing genetic and acquired disorders by introducing therapeutic nucleic acids into cells to correct, inhibit, or augment specific gene functions.[23–27] Diverse genetic therapeutic agents have been effectively employed for efficient and secure cellular transfection.[28–31] Nonetheless, obstacles such as cellular resistance and the pronounced negative charge of nucleic acids

[a]*Department of Chemistry, College of Science, Imam Mohammad Ibn Saud Islamic University (IMSIU), Riyadh 11623, Saudi Arabia*

[b]*Department of Biochemistry and Biophysics, Stockholm University, Stockholm 10691, Sweden*

[c]*Professor Emeritus, University of Tartu, Estonia*

[d]*Interdisciplinary Research Center for Hydrogen Technologies and Carbon Management, King Fahd University of Petroleum and Minerals (KFUPM), Dhahran, 31261, Saudi Arabia. E-mail: moataz.dowaidar@kfupm.edu.sa*

[e]*Bioengineering Department, King Fahd University of Petroleum and Minerals (KFUPM), Dhahran 31261, Saudi Arabia*

frequently impede the transfection efficiency.[32] To surmount these obstacles, both viral and non-viral vectors have been engineered.[33–39] Cell-penetrating peptides (CPPs) have garnered considerable interest among non-viral methods for their capacity to penetrate cellular membranes and transport various biomolecular cargoes straight into the cytoplasm or nucleus.[40,41] They are short peptides, generally including fewer than 30 amino acids, that can facilitate the translocation of nucleic acids, proteins, and tiny molecules into cells without requiring receptors or energy-dependent mechanisms.[42–47] Professor Ülo Langel, acknowledged as the foremost authority in CPP research, introduced the transportan peptide, one of the earliest and most extensively examined CPPs, and clarified the mechanisms of CPP-mediated internalization, significantly enhancing their biological applicability.[48,49] Notwithstanding their versatility, CPPs encounter numerous constraints, including low cargo selectivity, restricted serum stability, fast *in vivo* clearance, and possible cytotoxicity at high dosages. Furthermore, endosomal entrapment of CPP–cargo complexes frequently decreases bioavailability and transfection efficacy. Recent improvements indicate that nanoparticle conjugation can significantly augment CPP-mediated gene delivery and enhance the overall transfection efficacy.[50]

Herein, the complexation of CDs and GQDs with CPPs, PF-14 and PF221, for gene transfection is reported. The polyplex formation was achieved *via* complex formation between nanoparticles (CDs or GQDs), PF-14/PF-221, and gene therapeutic agents (*e.g.*, plasmid (pGL3, Luciferase Reporter Vectors) and splice correction oligonucleotides (SCO)). The pGL3 vector is a plasmid frequently utilized to investigate gene expression and promoter activity in molecular biology. Due to its high sensitivity, ease of use, and compatibility with mammalian cells, the pGL3 vector is a reliable tool for investigating gene regulation, signal transduction pathways, and transcriptional responses *in vitro*. Conversely, SCOs are small antisense nucleic acid sequences that influence pre-mRNA splicing by binding to specific splice sites or regulatory regions. They have demonstrated significant potential in treating genetic illnesses.[51]

Experimental

Materials and methods

Ascorbic acid was obtained from Sigma-Aldrich (Germany). Graphite was purchased from Alfa-Aesar (Germany). A luciferase-expressing plasmid (pGL3, 3 MDa) was purchased from Promega (Sweden). SCO (6.5 kDa) was obtained from Microsynth AG (Switzerland). Human glioblastoma cell line (U87 MG-luc2) was purchased from Caliper LifeSciences, USA. The chemicals were used without purification.

Synthesis of carbon dots (CDs)

CDs were prepared *via* the solvothermal method. A solution of ascorbic acid was prepared by dissolving 1 g in 10 mL of water using ultrasonic vibrations for 30 minutes. The solution was placed in an autoclave and heated at a temperature of 180 °C for 24 hours. Upon cooling, the CDs were obtained as a brown–yellow substance. The CD solution was subsequently refined through filtration using nitrocellulose filters (0.22 μm).

Synthesis of graphene oxide quantum dots (GQDs)

Following our previous procedures, graphite oxide was prepared using Hummers' method.[52–56] The graphite oxide (200 mg) was then stirred with sulfuric acid and nitric acid (50 mL) for 12 h at 30 °C. The brown solution was decanted and neutralized with NaOH before dialysis in water to achieve neutrality.

Surface modification with chitosan was performed by dispersing GO QDs in a chitosan solution (1% acetic acid, 1 mg mL^{-1}). The solution was stirred at room temperature for 12 h.

Peptide and polyplex synthesis

Two types of CPPs, including PF221 (Stearyl-FLKLLKKFLFLKLLKKFL-amide) and PF14 (Stearyl-AGYLLGKL-LOOLAAAALOOLL-NH_2), were synthesized using Fmoc-based solid-phase peptide synthesis on a SYRO II synthesizer (Multi-SynTech, Germany) with the Rink-amide resin (PCAS BioMatrix, Canada).[57,58]

For complex formation, a solution containing 80 μL of Milli-Q water, 4 μL of carbon nanoparticles (either CDs or GQDs, 1 mg mL^{-1}), 10.5 μL of SCO (10 μM), and 10.5 μL of each CPP (PF220–PF224 and PF14) was mixed sequentially and incubated at room temperature for 2 hours.

Cell culture and treatment

HeLa cells (7000 cells in 100 μL per well, 96-well plate) were used as the model system and cultured in DMEM supplemented with 1 mM sodium pyruvate, 1 mM glutamate, 0.1 mM non-essential amino acids, 10% fetal bovine serum (FBS), 100 U mL^{-1} penicillin, and 100 mg mL^{-1} streptomycin (Invitrogen, Sweden). HeLa puLc 705 cells (from Prof. R. Kole) and U-87 MG-luc2 cells were cultured at 37 °C and 5% CO_2 under similar conditions, with the addition of 200 U mL^{-1} of penicillin and 200 mg mL^{-1} of streptomycin.

Assessment of polyplex efficacy

To evaluate CPP-mediated delivery, 10 μL of CPP-pGL3-CDs or GQDs (using PF221 or PF14) was added to the HeLa cells (7000 cells per well), and the pGL3 luciferase expression was measured after 24 h using the GLOMAX™ luminometer (Promega, USA). For splice correction oligonucleotide (SCO) assays, HeLa puLc 705 cells were treated with CPP–SCO–CDs or GQDs complexes, lysed using 0.2% Triton X-100 in HKR buffer, and the luminescence was quantified.

SCARA inhibition studies

To investigate the role of scavenger receptor A (SCARA), HeLa 705 cells were pre-treated for 1 h with specific inhibitors named polyinosinic acid (poly I, 10 μg mL^{-1}), dextran sulfate (Dex, 2.5 μg mL^{-1}), and fucoidan (Fuc, 2.5 μg mL^{-1}) or control agents—polycytidylic acid (poly C), chondroitin sulfate (Chon), and galactose (Gal), at the same concentrations. Subsequently, 10 μL of the PF14–SCO or PF14–SCO–CD complex was added. After

24 h, luminescence measurements were taken and normalized to the highest activity observed for PF14–SCO-treated cells.

Instruments

Transmission electron microscopy (TEM) was performed using a JEM-2000FX microscope (JEOL, Japan) operating at an accelerating voltage of 200 kV. Samples were prepared by dropping the nanoparticle suspension onto 3 mm carbon-coated copper grids, which were then dried on filter paper. X-ray diffraction (XRD) analysis of the bare carbon nanoparticles was carried out using a PANalytical X'Pert diffractometer (PANalytical, Germany) operating at 45 kV and 40 mA to determine the crystallinity and phase structure. Zeta potential measurements were conducted using a Zetasizer Nano ZS particle analyzer (Malvern Instruments Ltd, UK) at 25 °C. The instrument was equipped with a 532 nm solid-state He–Ne laser, and measurements were taken at a fixed backscattering angle of 173° to assess the surface charge and colloidal stability of the nanoparticles.

Results and discussion

Materials synthesis and characterization

GO QDs were synthesized *via* a two-step process (Fig. 1a). Initially, GO was prepared using the modified Hummers' method, where graphite was oxidized in concentrated sulfuric acid with potassium permanganate, and water and hydrogen peroxide were carefully added to complete the reaction. The obtained graphite oxide was then dispersed in a mixed acid solution of sulfuric and nitric acids and stirred at 30 °C for 12 hours (Fig. 1a). This oxidative treatment facilitated the cutting of large GO sheets into smaller fragments, *i.e.*, the formation of GO QDs. The resulting brown dispersion was neutralized using sodium hydroxide and dialyzed against water to remove acid residues, yielding GO QDs (Fig. 1a).

CDs were produced through a green, solvothermal approach using ascorbic acid as a carbon precursor (Fig. 1b). Specifically, ascorbic acid was dissolved in distilled water by ultrasonication for 30 minutes to ensure complete dissolution. The solution was subjected to hydrothermal treatment. After natural cooling, a brown–yellow aqueous solution containing CDs was obtained. The CDs were purified using 0.22 μm nitrocellulose membrane filtration to remove unreacted precursors or large particles (Fig. 1b).

Two amphiphilic CPPs: PF221 and PF14, were synthesized using Fmoc solid-phase peptide synthesis on a SYRO II peptide synthesizer (Fig. 1c). These CPPs formed polyplexes with gene therapeutic cargos, *e.g.*, SCO or pGL3, and carbon nanomaterials (CDs or GO QDs). The components were mixed in Milli-Q water, a carbon nanoparticle solution, SCO or pGL3 plasmid, and CPP (PF221 or PF14) to prepare the polyplexes. The mixture was incubated at room temperature for 2 hours to facilitate electrostatic and hydrophobic interactions, allowing for stable nanocomplex formation. These complexes were then used in cell transfection assays for gene therapy applications. The materials were characterized by XRD (Fig. 2), TEM (Fig. 3), and zeta potential measurements (Fig. 4).

XRD patterns for the prepared carbon nanomaterials are plotted in Fig. 2. Fig. 2 displays XRD patterns of graphite, GO QDs, and CDs, highlighting the structural transformations resulting from the synthesis procedures. Graphite shows sharp

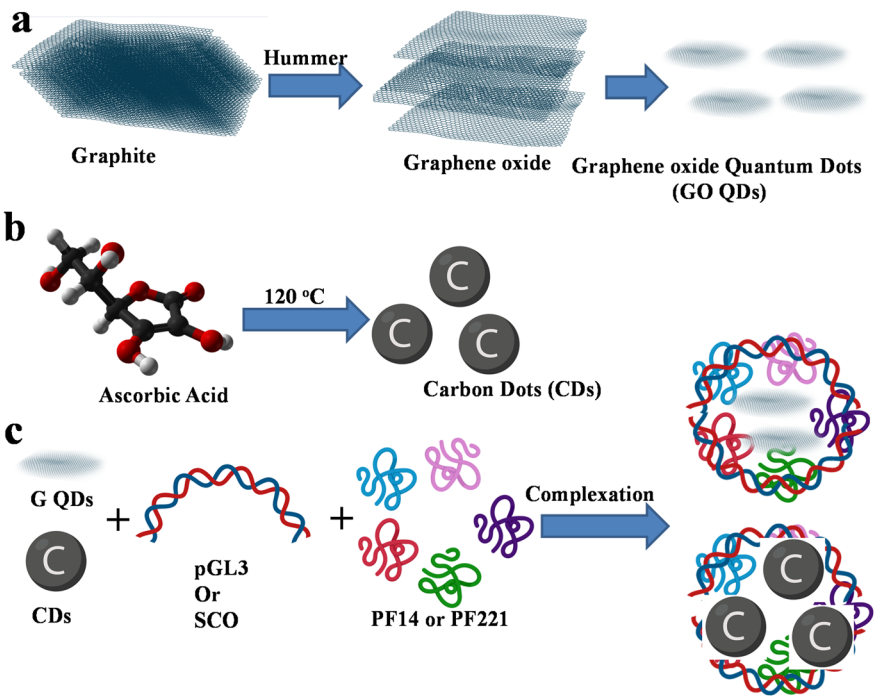

Fig. 1 Synthesis procedure for (a) GO QDs, (b) CDs, and (c) polyplexes of CPPs with carbon nanoparticles and gene therapeutic agents, namely, SCO or pGL3.

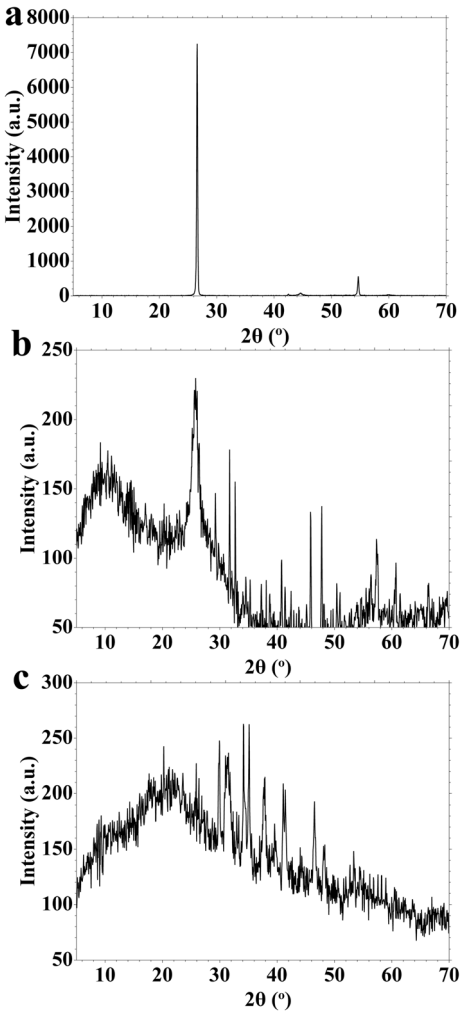

Fig. 2 XRD patterns of (a) graphite, (b) GO QDs, and (c) CDs.

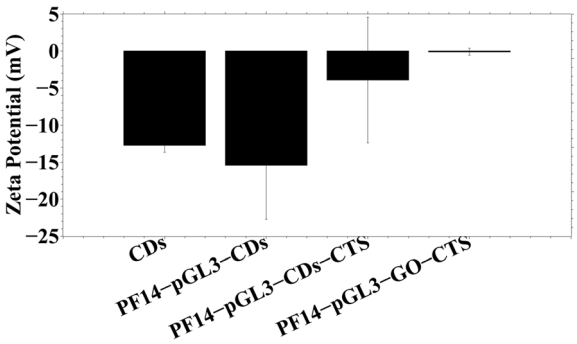

Fig. 4 Zeta potential for different polyplexes.

and well-defined peaks at $2\theta = 26.6°$ and 54.6°, corresponding to the (002) and (004) crystal planes of highly ordered graphitic layers (Fig. 2a), respectively. These reflections are characteristic of a well-crystallized sp^2-hybridized carbon lattice with regular interlayer spacing. GO QDs (Fig. 2b) exhibit two prominent peaks at 10.2° and 25° (Fig. 2b). The prominent peak at 10.2° is associated with the (001) plane of oxidized graphene layers, indicating increased interlayer spacing due to the introduction of oxygen-containing functional groups. The peak at 25° may result from graphitic domains. CDs display a broad, single peak centered around 20.1°, reflecting carbon dots' amorphous or poorly crystalline nature (Fig. 2c). This broadening is typical for CDs, which consist of small, disordered carbon clusters with a high surface-to-volume ratio and abundant surface functional groups. The noisy signals observed in GO QDs and CDs can be attributed to their low crystallinity, small particle sizes, and structural heterogeneity (Fig. 2b and c). Unlike graphite, these nanomaterials lack long-range order, and their surfaces are rich in defects and functional groups that disrupt regular stacking

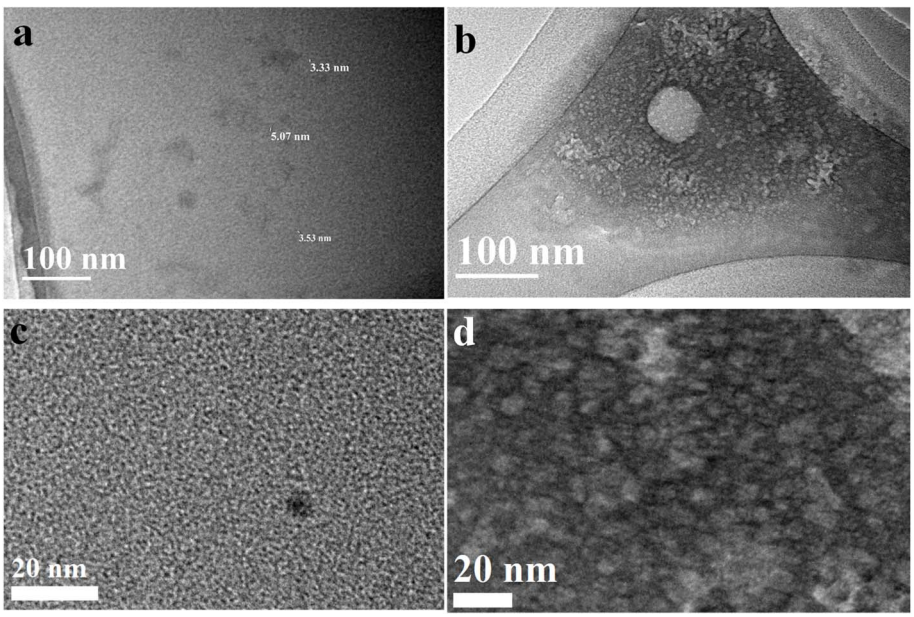

Fig. 3 TEM images of (a and b) CDs and (c and d) the CD–SCO–PF14 polyplex.

(Fig. 2a). Additionally, the nanoscale dimensions of GO QDs and CDs limit coherent scattering domains, further reducing diffraction intensity and contributing to baseline noise in the XRD patterns (Fig. 2).

Fig. 3 presents TEM images of CDs and their polyplex formed with SCO and PF14. Fig. 3a and b displays the morphology of pristine CDs, while Fig. 3c and d show the corresponding polyplex. CDs, which appear as uniform spherical nanoparticles with a narrow size distribution ranging from 1 to 2 nm, consistent with their ultrasmall size and amorphous carbon structure (Fig. 3a and b). High-resolution TEM (HR-TEM) confirms their monodispersity and fine crystallite-like features, often associated with short-range ordering within CDs (Fig. 3a and b). The polyplex of PF-14–SCO–CDs reveals a significant change in morphology (Fig. 3c and d). The images show bigger, aggregated structures decorated with discrete CD nanoparticles, suggesting complexation between CDs, SCO, and PF14. These assemblies are interpreted as polyplexes, in which the CDs are surrounded by a matrix of SCO and CPPs, forming a condensed nanostructure (Fig. 3c and d). These biomolecules introduce voids and irregularities into the structure, visible as light contrast regions in the TEM images (Fig. 3). The TEM analysis confirms the complexation of oligonucleotides within the CPP–CD nanocarriers.

The charge of the polyplex plays an essential role in gene transfection. Thus, the polyplexes were characterized using zeta potential measurements (Fig. 4). Fig. 4 illustrates the zeta potential values of various carbon nanoparticle-based polyplex formulations: pristine CDs (−12.7 mV), PF14-pGL3-CDs (−15.4 mV), PF14-pGL3-CDs-CTS (−3.9 mV), and PF14-pGL3-GO-CTS (−0.09 mV). These measurements provide critical insights into the surface charge characteristics and colloidal stability of the nanocomplexes, which play a vital role in their cellular uptake and transfection efficiency. CDs exhibit a moderately negative charge of −12.7 mV due to their surface functional groups (*e.g.*, carboxyl and hydroxyl), typical for ascorbic acid-derived CDs. PF14-pGL3-CDs polyplexes show a slightly more negative charge (−15.4 mV), likely due to the electrostatic contribution of the anionic pGL3 plasmid DNA, which dominates the net surface potential despite the presence of the positively charged PF14 peptide. Upon the addition of chitosan (CTS) to the polyplex (PF14-pGL3-CDs-CTS), the zeta potential shifts significantly towards neutrality (−3.9 mV, Fig. 4). Chitosan, a cationic polysaccharide, partially neutralizes the negative charges, improving surface properties for cell membrane interaction and endosomal escape. PF14-pGL3-GO-CTS exhibits a nearly neutral zeta potential (−0.09 mV), suggesting strong charge shielding by chitosan around the GO QD core and cargo.

CDs are small carbon-based materials with abundant hydroxyl, carboxyl, and amine functional groups on their surfaces, which can effectively interact with oligonucleotides and CPPs through noncovalent interactions. The interaction between CDs and oligonucleotides is primarily governed by electrostatic attraction, as the positively charged amine groups on CDs bind with the negatively charged phosphate backbone of DNA or RNA. Furthermore, hydrogen bonding between the hydroxyl or carboxyl groups of cyclodextrins and the nucleobases or phosphate oxygen atoms further stabilizes the complex, enabling cyclodextrins to serve as carriers that protect oligonucleotides from degradation and improve their cellular transit. Similarly, CDs can form stable complexes with CPPs, often rich in positively charged amino acids, such as lysine and arginine. In this scenario, electrostatic interactions occur between the negatively charged carboxyl groups of CDs and the cationic residues of CPPs, while the hydrogen bonding between the functional groups of CDs and the peptide backbone or side chains strengthens the contact. These noncovalent interactions collectively enhance the attachment of CDs with oligonucleotides and CPPs, making them appealing nanocarriers for gene and peptide delivery in biomedical applications.

Gene transfection

Gene transfections of the pGL3 plasmid (Fig. 5) and SCO (Fig. 6) have been investigated. Fig. 5 illustrates the transfection efficiency (% relative expression) of the pGL3 plasmid in cells delivered *via* polyplexes formed with two different CPPs, *e.g.*, PF14 and PF221, in combination with various carbon nanomaterials (GO QDs and CDs), with or without chitosan (CTS). PF14-pGL3-CDs exhibited the highest transfection efficiency, significantly surpassing all other groups. The high performance suggests that CDs, when combined with PF14, provide an optimal environment for pGL3 delivery, likely due to their small size, high surface area, and favorable charge distribution. PF14-pGL3-GO Qdots and PF14-pGL3-GO Qdots CTS showed moderate efficiencies, slightly lower than those of the CD-based complexes. The low efficiency may be due to the relatively larger size of GO QDs and their planar structure, which might affect complex formation or cellular uptake. PF14-pGL3-CDs-CTS reduced transfection compared to their non-chitosan counterpart (Fig. 5a). Although CTS can enhance cellular uptake in some systems, in this case, it might hinder gene release or interfere with cellular trafficking. PF14-pGL3 alone (without nanoparticles) showed moderate efficiency, confirming that carbon nanoparticles improve transfection by stabilizing the polyplex and aiding endocytosis.

The transfection efficiencies of the PF-221 groups are overall lower than those of the PF14 group, suggesting that PF-221 is less effective than PF14 for this delivery system (Fig. 5b). PF221-pGL3-GO Qdots and CTS-functionalized GO Qdots showed the highest expression levels among PF221-based systems, but still did not outperform the PF14–CDs system (Fig. 5b). PF221–CD complexes yielded lower transfection than GO QDs, indicating that the CPP-nanomaterial compatibility is critical in determining delivery efficiency. PF14 in combination with CDs is the most efficient delivery system for the pGL3 plasmid among the tested groups. The CPP choice significantly affects performance. PF14 outperforms PF221, possibly due to differences in membrane interactions, internalization, or endosomal escape. Chitosan modification can modulate the transfection efficiency, but its impact is context-dependent, requiring optimization for each carrier-peptide system.

Fig. 6 illustrates the transfection efficiency of SCO utilizing PF14 (Fig. 6a) and PF221 (Fig. 6a), using various carbon-based

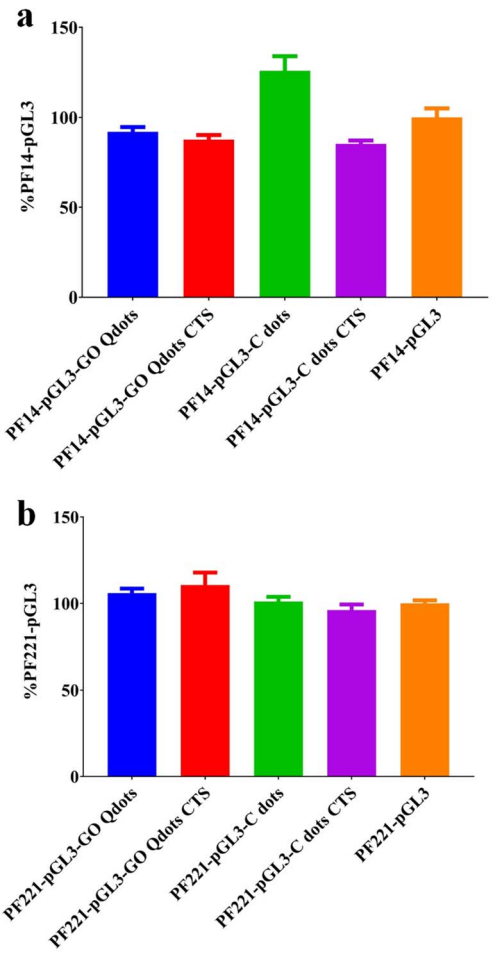

Fig. 5 Cell-transfection efficiency for the pGL3 plasmid using (a) PF-14 and (b) PF-221.

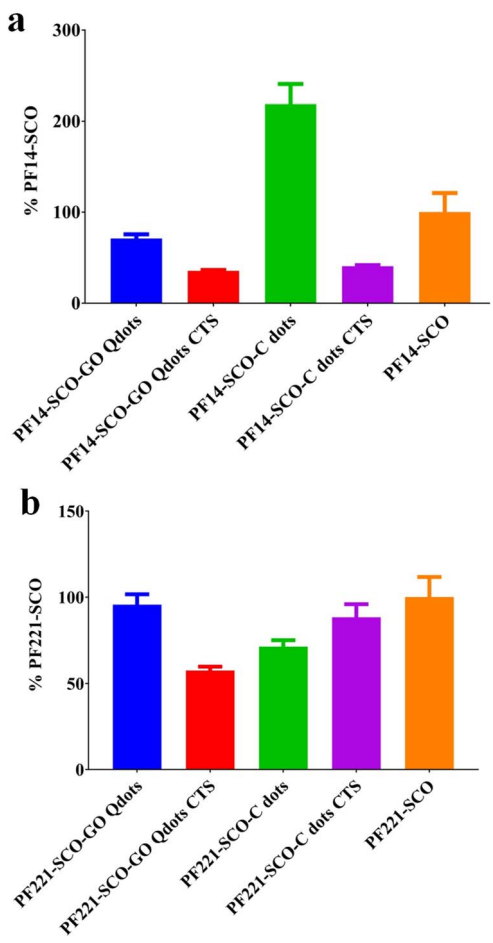

Fig. 6 Cell transfection efficiency for SCO using (a) PF-14 and (b) PF-221.

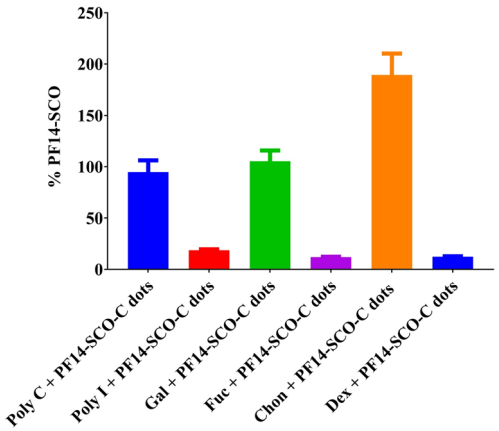

Fig. 7 Mechanism for cell uptake or transfection using the scavenger receptor class.

nanocarriers, such as GO Qdots and CDs, with or without CTS modification. In the PF14-based systems, the PF14–SCO–CD formulation exhibited the highest transfection efficiency, exceeding 220% (Fig. 6a). The high efficiency suggests a robust synergistic interaction between PF14 and CDs, possibly attributable to the carbon dots' large surface area and nanoscale dimensions, which enhance cellular absorption and effective SCO delivery. Conversely, PF14–SCO alone and PF14–SCO–GO Qdots exhibited moderate transfection efficiencies of around 100% and 75%, indicating that, although PF14 alone is successful, the incorporation of CDs significantly augments its transport capability (Fig. 6a). The PF14–SCO–CDs CTS and PF14–SCO–GO Qdot CTS formulations exhibited the lowest transfection efficiencies, suggesting that chitosan may impede cellular uptake or delay SCO release, either due to steric hindrance or adverse modifications in surface charge (Fig. 6a).

In PF221-based systems, all formulations demonstrated reduced transfection efficiency relative to PF14 (Fig. 6b). The maximum efficiency was noted for PF221–SCO–GO Qdots, almost equivalent to PF221–SCO alone, indicating that GO Qdots do not substantially improve SCO delivery for PF221. With or without chitosan, formulations using CDs exhibited minor enhancement, ranging from 70% to 90%, suggesting a low interaction or compatibility between PF221 and the CDs. The persistent deterioration in the performance of CTS-modified systems across both CPP types substantiates the assertion that CTs hinder optimum interaction and adsorption, presumably due to modifications in the particle surface charge and structure. Again, the results indicate that PF14 is a superior

Table 1 Summary of the nanoparticles used for CPP-ON delivery

Nanoparticle system	CPPs used	Gene cargo	Fold improvement	Ref.
ZIF-8	PFs (general)	Plasmid, SCO, siRNA	2–8 fold	57
MPC (from chitosan@ZIF-8)	PF14 PF221	Plasmid, SCO	Up to 10 fold	58
GO	PF14, PF221	Plasmid	2.1–2.5 fold	61
	PF14	SCO	>10–25 fold	
MNPs (Fe_3O_4)	PF14	Plasmid, SCO, siRNA	Up to 4 fold	62
CTS@MNPs	PF14	Plasmid, SCO, siRNA	Up to 6 fold (*vs.* PF14 alone)	63
PF14–SCO-MNPs	PF14	SCO	Outperformed Lipofectamine™ 2000	63
CDs	PF14	pGL3 SCO	2.0–2.1	This work

cell compared to PF221 for the delivery of SCO, especially in conjunction with CDs.

The cell uptake mechanism was investigated using the scavenger receptor class (Fig. 7). Fig. 7 examines the cellular absorption and transfection method of PF14–SCO–CD polyplexes, emphasizing the role of scavenger receptor class A (SCARA). The precise internalization mechanism of the CPP-oligonucleotide (ON) complexes is not fully understood; however, various potential mechanisms have been suggested, including endocytosis, energy-independent translocation,[59] and SCARA-mediated uptake.[60] SCARA operates as a pattern recognition receptor that can bind and internalize acetylated low-density lipoproteins, positioning it as a probable mediator for the uptake of CPP-based complexes. To investigate the function of SCARA, HeLa cells were preincubated with established inhibitors, dextran sulfate (Dex), polyinosinic acid (Poly I), and fucoidin (Fuc), alongside structurally analogous control compounds, *e.g.*, chondroitin sulfate (Chon), polycytidylic acid (Poly C), and galactose (Gal)—that do not interact with SCARA (Fig. 7). Fig. 7 indicates that Dex, Poly I, and Fuc significantly impede the transfection effectiveness of PF14–SCO–CDs, with Dex and Fuc decreasing it by more than 90%, highlighting SCARA's pivotal involvement in cellular internalization. Conversely, the control substances, Chon, Poly C, and Gal, demonstrated negligible to no inhibition, hence affirming the specificity of the observed effects. The data indicate that SCARA-mediated endocytosis is the primary mechanism for the internalization of PF14–SCO–CDs. The substantial reduction in transfection efficiency following SCARA inhibitor treatment substantiates the concept that SCARA is essential for the uptake of CPP–SCO complexes, consistent with prior findings on analogous nanoparticle systems. Nevertheless, although the data compellingly indicate SCARA, they do not exclude the possible involvement of other prevalent endocytic routes, such as clathrin-mediated endocytosis, caveolae-dependent uptake, or macropinocytosis, which are also commonly associated with CPP and nanoparticle uptake. A thorough mechanistic analysis with specific inhibitors of clathrin (*e.g.*, chlorpromazine), caveolae (*e.g.*, nystatin or filipin), and macropinocytosis (*e.g.*, EIPA) might elucidate the potential contributions of these pathways in conjunction with SCARA. Additional experiments could be added to reinforce the finding that SCARA is the primary absorption pathway for PF14–SCO–CDs and eliminate or quantify the contributions of alternative mechanisms.

Nanoparticles improve the cell transfection of CPPs (Table 1). They emphasize the synergistic application of CPPs, including PepFects (*e.g.*, PF14, PF221, PF220), in conjunction with nanomaterials, to improve non-viral gene delivery (Table 1). Nanocarriers, such as zeolitic imidazolate frameworks (ZIF-8) and their composites (*e.g.*, BSA@ZIF-8, RhB@ZIF-8, GO@ZIF-8, MNPs@ZIF-8),[57] mesoporous carbon (MPC) derived from chitosan-encapsulated ZIF-8,[58] graphene oxide (GO),[61] and magnetic nanoparticles (MNPs),[62,63] exhibit enhanced transfection efficiencies for plasmid DNA, SCO, and small interfering RNA (siRNA). These systems exhibit significant biocompatibility, minimal cytotoxicity, and effective cellular uptake, primarily facilitated by SCARA pathways. Integrating CPPs with nanomaterials markedly improves gene delivery efficacy by 2 to 25-fold, contingent upon the system and payload, surpassing conventional CPP-only methods or commercial vectors, such as Lipofectamine™ 2000 (Table 1).

Conclusions

This study demonstrates the efficacy of carbon-based nanocarriers, specifically CDs, for effective and targeted gene delivery when combined with amphiphilic cell-penetrating peptides, such as PF14. Among all evaluated systems, PF14–CDs polyplexes demonstrated enhanced transfection effectiveness for plasmid DNA and splice-correcting oligonucleotides, attributed to their advantageous nanoscale shape, appropriate surface charge, and high compatibility with the therapeutic cargo. Structural analysis confirmed the formation of polyplexes, whereas mechanistic investigations highlighted the essential role of scavenger receptor class A (SCARA) in facilitating cellular uptake. Compared to PF221, PF14 demonstrated superior distribution efficiency, underscoring the importance of peptide selection in constructing efficient nanocarriers. These results lay the foundation for scalable, adjustable gene-delivery systems using biocompatible carbon nanomaterials and cell-penetrating peptides for gene-based therapeutic applications.

Conflicts of interest

The authors declare that they have no known competing financial interests or personal relationships that could have appeared to influence the work reported in this paper.

Data availability

The datasets generated and analyzed during the current study are available from the corresponding author upon reasonable request. AI tools were only used for language improvement and content structuring. All scientific interpretations, analyses, and conclusions are the authors' sole responsibility.

Acknowledgements

The authors wish to express thanks for the financial support received from the Interdisciplinary Research Center for Hydrogen Technologies and Carbon Management, King Fahd University of Petroleum and Minerals (KFUPM), (Project No. INHE2302), Dhahran, 31261, Saudi Arabia.

References

1 M. Jiang, Y. Sun, M. Chen, H. Ji, Y. Liu, R. Qin, X. Li, H. Gao, R. Zhang and L. Zhang, Multicolor luminescence of carbon Dots: From mechanisms to applications, *Chem. Eng. J.*, 2024, **496**, 153761, DOI: 10.1016/j.cej.2024.153761.

2 P. Tian, L. Tang, K. S. Teng and S. P. Lau, Graphene quantum dots from chemistry to applications, *Mater. Today Chem.*, 2018, **10**, 221–258, DOI: 10.1016/j.mtchem.2018.09.007.

3 H. N. Abdelhamid, N, S-Doped Carbon Dots (N, S-CDs) for Perfluorooctane Sulfonic Acid (PFOS), *Detection*, 2025, **11**, 36, DOI: 10.3390/c11020036.

4 H. N. Abdelhamid, Organic-based nanostructure for chemosensors and biosensors: A review, *Microchem. J.*, 2025, **215**, 114383, DOI: 10.1016/j.microc.2025.114383.

5 F. K. Algethami and H. N. Abdelhamid, Heteroatoms-doped carbon dots as dual probes for heavy metal detection, *Talanta*, 2024, **273**, 125893, DOI: 10.1016/j.talanta.2024.125893.

6 H. N. Abdelhamid, A. Talib and H.-F. Wu, One pot synthesis of gold – carbon dots nanocomposite and its application for cytosensing of metals for cancer cells, *Talanta*, 2017, **166**, 357–363, DOI: 10.1016/j.talanta.2016.11.030.

7 M. Alafeef, I. Srivastava, T. Aditya and D. Pan, Carbon Dots: From Synthesis to Unraveling the Fluorescence Mechanism, *Small*, 2023, **20**(4), 2303937, DOI: 10.1002/smll.202303937.

8 X.-H. Hu and X. An, Green synthesis of fluorescent carbon dots from ascorbic acid and their application in sensing and biological imaging, *Next Mater.*, 2024, **4**, 100226, DOI: 10.1016/j.nxmate.2024.100226.

9 H. Liu, X. Zhong, Q. Pan, Y. Zhang, W. Deng, G. Zou, H. Hou and X. Ji, A review of carbon dots in synthesis strategy, *Coord. Chem. Rev.*, 2024, **498**, 215468, DOI: 10.1016/j.ccr.2023.215468.

10 H. N. Abdelhamid, An introductory review on advanced multifunctional materials, *Heliyon*, 2023, e18060, DOI: 10.1016/j.heliyon.2023.e18060.

11 X. Zhao, W. Gao, H. Zhang, X. Qiu and Y. Luo, Graphene quantum dots in biomedical applications: recent advances and future challenges, *Handbook of Nanomaterials in Analytical Chemistry* Elsevier, 2020, pp. 493–505, DOI: 10.1016/B978-0-12-816699-4.00020-7.

12 Z. Yu, F. Li and Q. Xiang, Carbon dots-based nanocomposites for heterogeneous photocatalysis, *J. Mater. Sci. Technol.*, 2024, **175**, 244–257, DOI: 10.1016/j.jmst.2023.08.023.

13 S. Zhu, Q. Meng, L. Wang, J. Zhang, Y. Song, H. Jin, K. Zhang, H. Sun, H. Wang and B. Yang, Highly Photoluminescent Carbon Dots for Multicolor Patterning, Sensors, and Bioimaging, *Angew. Chem., Int. Ed.*, 2013, **52**, 3953–3957, DOI: 10.1002/anie.201300519.

14 M. Bartkowski, Y. Zhou, M. Nabil Amin Mustafa, A. J. Eustace and S. Giordani, CARBON DOTS: Bioimaging and Anticancer Drug Delivery, *Chem.–Eur. J.*, 2024, **30**(19), e202303982, DOI: 10.1002/chem.202303982.

15 Z. Zahed, R. Hadi, G. Imanzadeh, Z. Ahmadian, S. Shafiei, A. Z. Zadeh, H. Karimi, A. Akbarzadeh, M. Abbaszadeh, L. S. Ghadimi, H. S. Kafil and F. Kazeminava, Recent advances in fluorescence nanoparticles "quantum dots" as gene delivery system: A review, *Int. J. Biol. Macromol.*, 2024, **254**, 127802, DOI: 10.1016/j.ijbiomac.2023.127802.

16 C. Liu, X. Lin, J. Liao, M. Yang, M. Jiang, Y. Huang, Z. Du, L. Chen, S. Fan and Q. Huang, Carbon dots-based dopamine sensors: Recent advances and challenges, *Chinese Chem. Lett.*, 2024, **35**, 109598, DOI: 10.1016/j.cclet.2024.109598.

17 M. Tuerhong, Y. XU and X.-B. YIN, Review on Carbon Dots and Their Applications, *Chinese J. Anal. Chem.*, 2017, **45**, 139–150, DOI: 10.1016/S1872-2040(16)60990-8.

18 A. Selva Sharma and N. Y. Lee, Comprehensive review on fluorescent carbon dots and their applications in nucleic acid detection, nucleolus targeted imaging and gene delivery, *Analyst*, 2024, **149**, 4095–4115, DOI: 10.1039/D4AN00630E.

19 Y. Wang, Z. Gu, J. Dong, J. Zhu, C. Liu, G. Li, M. Lu, J. Han, S. Cao, L. Chen and W. Wang, Green synthesis of chlorella-derived carbon dots and their fluorescence imaging in zebrafish, *RSC Adv.*, 2024, **14**, 1459–1463, DOI: 10.1039/D3RA07623G.

20 Z. Kang and S.-T. Lee, Carbon dots: advances in nanocarbon applications, *Nanoscale*, 2019, **11**, 19214–19224, DOI: 10.1039/C9NR05647E.

21 J. Li and X. Gong, The Emerging Development of Multicolor Carbon Dots, *Small*, 2022, **18**(51), 2205099, DOI: 10.1002/smll.202205099.

22 M. Chen, J. Ma, Y. Feng, Y. Wu, G. Hu and X. Liu, Advanced characterization enables a new era of efficient carbon dots electrocatalytic reduction, *Coord. Chem. Rev.*, 2025, **535**, 216612, DOI: 10.1016/j.ccr.2025.216612.

23 A. Schambach, C. J. Buchholz, R. Torres-Ruiz, K. Cichutek, M. Morgan, I. Trapani and H. Büning, A new age of precision gene therapy, *Lancet*, 2024, **403**, 568–582, DOI: 10.1016/S0140-6736(23)01952-9.

24 S. Tan, C. Yuan, Y. Zhu, S. Chang, Q. Li, J. Ding, X. Gao, R. Tian, Z. Han and Z. Hu, Glutathione hybrid poly (beta-amino ester)-plasmid nanoparticles for enhancing gene

delivery and biosafety, *J. Adv. Res.*, 2025, **73**, 697–711, DOI: 10.1016/j.jare.2024.07.038.

25 W. Zou, B. Huo, Y. Tu, Y. Zhu, Y. Hu, Q. Li, X. Yu, B. Liu, W. Tang, S. Tan and H. Xiao, Metabolic reprogramming by chemo-gene co-delivery nanoparticles for chemo-immunotherapy in head and neck squamous cell carcinoma, *Acta Biomater.*, 2025, **199**, 361–373, DOI: 10.1016/j.actbio.2025.04.031.

26 H. Liu, Z. Guo and P. Wang, Genetic expression in cancer research: Challenges and complexity, *Gene Rep.*, 2024, **37**, 102042, DOI: 10.1016/j.genrep.2024.102042.

27 F. Tang, A. Ding, Y. Xu, Y. Ye, L. Li, R. Xie and W. Huang, Gene and Photothermal Combination Therapy: Principle, Materials, and Amplified Anticancer Intervention, *Small*, 2024, **20**(6), 2307078, DOI: 10.1002/smll.202307078.

28 M. Chehelgerdi, M. Chehelgerdi, M. Khorramian-Ghahfarokhi, M. Shafieizadeh, E. Mahmoudi, F. Eskandari, M. Rashidi, A. Arshi and A. Mokhtari-Farsani, Comprehensive review of CRISPR-based gene editing: mechanisms, challenges, and applications in cancer therapy, *Mol. Cancer*, 2024, **23**, 9, DOI: 10.1186/s12943-023-01925-5.

29 E. Deneault, Recent Therapeutic Gene Editing Applications to Genetic Disorders, *Curr. Issues Mol. Biol.*, 2024, **46**, 4147–4185, DOI: 10.3390/cimb46050255.

30 K. Singh, P. Sethi, S. Datta, J. S. Chaudhary, S. Kumar, D. Jain, J. K. Gupta, S. Kumar, A. Guru and S. P. Panda, Advances in gene therapy approaches targeting neuro-inflammation in neurodegenerative diseases, *Ageing Res. Rev.*, 2024, **98**, 102321, DOI: 10.1016/j.arr.2024.102321.

31 M. Shine, J. Gordon, L. Schärfen, D. Zigackova, L. Herzel and K. M. Neugebauer, Co-transcriptional gene regulation in eukaryotes and prokaryotes, *Nat. Rev. Mol. Cell Biol.*, 2024, **25**, 534–554, DOI: 10.1038/s41580-024-00706-2.

32 H. Zhang, J. Vandesompele, K. Braeckmans, S. C. De Smedt and K. Remaut, Nucleic acid degradation as barrier to gene delivery: a guide to understand and overcome nuclease activity, *Chem. Soc. Rev.*, 2024, **53**, 317–360, DOI: 10.1039/D3CS00194F.

33 L. Dong, Y. Li, H. Cong, B. Yu and Y. Shen, A review of chitosan in gene therapy: Developments and challenges, *Carbohydr. Polym.*, 2024, **324**, 121562, DOI: 10.1016/j.carbpol.2023.121562.

34 J.-H. Wang, D. J. Gessler, W. Zhan, T. L. Gallagher and G. Gao, Adeno-associated virus as a delivery vector for gene therapy of human diseases, *Signal Transduct. Target. Ther.*, 2024, **9**, 78, DOI: 10.1038/s41392-024-01780-w.

35 B. Tafech, F. Mohabatpour and S. Hedtrich, Surface modification of lipid nanoparticles for gene therapy, *J. Gene Med.*, 2024, **26**(1), e3642, DOI: 10.1002/jgm.3642.

36 S. Yu, J. Zheng, H. Xie, Q. Deng, J. Wang, J. Chen, H. Zhou and J. Wang, Biocompatible Hydrogel Nanoparticles with Lysosomal Escape Properties for the Delivery of siRNA for the Gene Therapy of Colorectal Carcinoma, *ACS Appl. Nano Mater.*, 2024, **7**, 6626–6635, DOI: 10.1021/acsanm.4c00466.

37 Z. Wang, S. Pang, X. Liu, Z. Dong, Y. Tian, M. Ashrafizadeh, N. Rabiee, Y. N. Ertas and Y. Mao, Chitosan- and hyaluronic acid-based nanoarchitectures in phototherapy: Combination cancer chemotherapy, immunotherapy and gene therapy, *Int. J. Biol. Macromol.*, 2024, **273**, 132579, DOI: 10.1016/j.ijbiomac.2024.132579.

38 F. Farjadian, S. Mirkiani, P. Ghasemiyeh, H. Rahbar Kafshboran, S. Mehdi-Alamdarlou, A. Raeisi, R. Esfandiarinejad, S. Soleymani, G. Goshtasbi, N. Firouzabadi, S. Mohammadi-Samani, M. Hossein Morowvat and M. Doroudian, Smart nanogels as promising platform for delivery of drug, gene, and vaccine; therapeutic applications and active targeting mechanism, *Eur. Polym. J.*, 2024, **219**, 113400, DOI: 10.1016/j.eurpolymj.2024.113400.

39 Y. Liu, Z. Zhang, H. Du, X. Chen, N. Hu, T. Yu, M. Hou and X. Yu, An enzyme-responsive hydrogel functionalized with mesoporous silica nanoparticles for co-delivery of cisplatin and shRNA to overcome chemotherapy resistance in non-small cell lung cancer, *RSC Adv.*, 2025, **15**, 23966–23977, DOI: 10.1039/D5RA03250D.

40 M. Lindgren, M. Hällbrink, A. Prochiantz and Ü. Langel, Cell-penetrating peptides, *Trends Pharmacol. Sci.*, 2000, **21**, 99–103, DOI: 10.1016/S0165-6147(00)01447-4.

41 M. Pooga, U. Soomets, M. Hällbrink, A. Valkna, K. Saar, K. Rezaei, U. Kahl, J.-X. Hao, X.-J. Xu, Z. Wiesenfeld-Hallin, T. Hökfelt, T. Bartfai and Ü. Langel, Cell penetrating PNA constructs regulate galanin receptor levels and modify pain transmission in vivo, *Nat. Biotechnol.*, 1998, **16**, 857–861, DOI: 10.1038/nbt0998-857.

42 V. Guzman Gonzalez, A. Grunenberger, O. Nicoud, E. Czuba, J. Vollaire, V. Josserand, X. Le Guével, N. Desai, J.-L. Coll, G. Divita and V. Faure, Enhanced CRISPR-Cas9 RNA system delivery using cell penetrating peptides-based nanoparticles for efficient in vitro and in vivo applications, *J. Contr. Release*, 2024, **376**, 1160–1175, DOI: 10.1016/j.jconrel.2024.11.008.

43 C.-Y. Lin, J.-Y. Fang, C.-Y. Hsiao, C.-W. Lee, A. Alshetaili and Z.-C. Lin, Dual cell-penetrating peptide-conjugated polymeric nanocarriers for miRNA-205–5p delivery in gene therapy of cutaneous squamous cell carcinoma, *Acta Biomater.*, 2025, **196**, 332–349, DOI: 10.1016/j.actbio.2025.02.056.

44 X. Wang, C. Cai, W. Lv, K. Chen, J. Li, K. Liao, Y. Zhang, H. Huang, Y. Lin, Z. Rong and X. Duan, Short cell-penetration peptide conjugated bioreducible polymer enhances gene editing of CRISPR system, *J. Nanobiotechnol.*, 2024, **22**, 284, DOI: 10.1186/s12951-024-02554-w.

45 H. Feyzyab, A. Milani, E. Agi, M. Hashemi and A. Bolhassani, Investigation of the Potency of KALA and REV Cell-Penetrating Peptides for In Vitro/In Vivo Delivery of an HPV Multiepitope DNA Construct, *J. Pept. Sci.*, 2025, **31**(1), e70000, DOI: 10.1002/psc.70000.

46 R. Xu, C. Xia, X. He, C. Hu, Y. Li, Y. Zhang and Z. Chen, siRNA Nanoparticle Dry Powder Formulation with High Transfection Efficiency and Pulmonary Deposition for Acute Lung Injury Treatment, *ACS Appl. Mater. Interfaces*, 2024, **16**, 54344–54358, DOI: 10.1021/acsami.4c04241.

47 M. Pirhaghi, F. Mamashli, F. Moosavi-Movahedi, P. Arghavani, A. Amiri, B. Davaeil, M. Mohammad-Zaheri, Z. Mousavi-Jarrahi, D. Sharma, Ü. Langel, D. E. Otzen and A. A. Saboury, Cell-Penetrating Peptides: Promising Therapeutics and Drug-Delivery Systems for Neurodegenerative Diseases, *Mol. Pharm.*, 2024, **21**, 2097–2117, DOI: **10.1021/acs.molpharmaceut.3c01167**.

48 M. Pooga, M. Hällbrink, M. Zorko and Ü. Langel, Cell penetration by transportan, *FASEB J.*, 1998, **12**, 67–77, DOI: **10.1096/fj.1530-6860**.

49 M. Dowaidar, H. N. Abdelhamid and Ü. Langel, Improvement of Transfection with PepFects Using Organic and Inorganic Materials, *Methods Mol. Biol.*, 2022, 555–567, DOI: **10.1007/978-1-0716-1752-6_35**.

50 Y. Wei, H. Bao, L. Wang, Y. Cao, Z. Liu, X. Zhu, T. Chen, A. Wu and J. Li, Cell-Penetrating Peptides-Mediated Therapeutic Agents Delivery into the Central Nervous System, *ACS Mater. Lett.*, 2024, **6**, 2239–2258, DOI: **10.1021/acsmaterialslett.4c00397**.

51 J. Rytkönen, P. Arukuusk, W. Xu, K. Kurrikoff, Ü. Langel, V.-P. Lehto and A. Närvänen, Porous Silicon–Cell Penetrating Peptide Hybrid Nanocarrier for Intracellular Delivery of Oligonucleotides, *Mol. Pharm.*, 2014, **11**, 382–390, DOI: **10.1021/mp4002624**.

52 W. S. Hummers and R. E. Offeman, Preparation of Graphitic Oxide, *J. Am. Chem. Soc.*, 1958, **80**, 1339, DOI: **10.1021/ja01539a017**.

53 A. A. Sadek, M. Abd-Elkareem, H. N. Abdelhamid, S. Moustafa and K. Hussein, Repair of critical-sized bone defects in rabbit femurs using graphitic carbon nitride (g-C3N4) and graphene oxide (GO) nanomaterials, *Sci. Rep.*, 2023, **13**, 5404, DOI: **10.1038/s41598-023-32487-7**.

54 H. N. Abdelhamid and H.-F. Wu, A method to detect metal-drug complexes and their interactions with pathogenic bacteria via graphene nanosheet assist laser desorption/ionization mass spectrometry and biosensors, *Anal. Chim. Acta*, 2012, **751**, 94–104, DOI: **10.1016/j.aca.2012.09.012**.

55 H. Nasser Abdelhamid, B.-S. Wu and H.-F. Wu, Graphene coated silica applied for high ionization matrix assisted laser desorption/ionization mass spectrometry: A novel approach for environmental and biomolecule analysis, *Talanta*, 2014, **126**, 27–37, DOI: **10.1016/j.talanta.2014.03.016**.

56 H. N. Abdelhamid, M. S. Khan and H. F. Wu, Graphene oxide as a nanocarrier for gramicidin (GOGD) for high antibacterial performance, *RSC Adv.*, 2014, **4**, 50035–50046, DOI: **10.1039/c4ra07250b**.

57 H. N. Abdelhamid, M. Dowaidar, M. Hällbrink and Ü. Langel, Gene delivery using cell penetrating peptides-zeolitic imidazolate frameworks, *Microporous Mesoporous Mater.*, 2020, **300**, 110173, DOI: **10.1016/j.micromeso.2020.110173**.

58 H. N. Abdelhamid, M. Dowaidar and Ü. Langel, Carbonized chitosan encapsulated hierarchical porous zeolitic imidazolate frameworks nanoparticles for gene delivery, *Microporous Mesoporous Mater.*, 2020, **302**, 110200, DOI: **10.1016/j.micromeso.2020.110200**.

59 J. Müller, J. Triebus, I. Kretzschmar, R. Volkmer and P. Boisguerin, The agony of choice: how to find a suitable CPP for cargo delivery, *J. Pept. Sci.*, 2012, **18**, 293–301, DOI: **10.1002/psc.2396**.

60 K. Ezzat, H. Helmfors, O. Tudoran, C. Juks, S. Lindberg, K. Padari, S. El-Andaloussi, M. Pooga and U. Langel, Scavenger receptor-mediated uptake of cell-penetrating peptide nanocomplexes with oligonucleotides, *FASEB J.*, 2012, **26**, 1172–1180, DOI: **10.1096/fj.11-191536**.

61 M. Dowaidar, H. N. Abdelhamid, M. Hällbrink, X. Zou and Ü. Langel, Graphene oxide nanosheets in complex with cell penetrating peptides for oligonucleotides delivery, *Biochim. Biophys. Acta Gen. Subj.*, 2017, **1861**, 2334–2341, DOI: **10.1016/j.bbagen.2017.07.002**.

62 M. Dowaidar, H. N. Abdelhamid, M. Hällbrink, K. Kurrikoff, K. Freimann, X. Zou, Ü. Langel, K. Kurrikoff, X. Zou and Ü. Langel, Magnetic Nanoparticle Assisted Self-assembly of Cell Penetrating Peptides-Oligonucleotides Complexes for Gene Delivery, *Sci. Rep.*, 2017, **7**, 9159, DOI: **10.1038/s41598-017-09803-z**.

63 M. Dowaidar, H. Nasser Abdelhamid, M. Hällbrink, Ü. Langel and X. Zou, Chitosan enhances gene delivery of oligonucleotide complexes with magnetic nanoparticles–cell-penetrating peptide, *J. Biomater. Appl.*, 2018, **33**, 392–401, DOI: **10.1177/0885328218796623**.